Liang, Daolun; Liu, Jianzhong; Qiu, Qili

Article

Nano carbides-mediated acceleration of energy release behavior of amorphous boron during ignition and combustion

Energy Reports

Provided in Cooperation with:
Elsevier

Suggested Citation: Liang, Daolun; Liu, Jianzhong; Qiu, Qili (2020) : Nano carbides-mediated acceleration of energy release behavior of amorphous boron during ignition and combustion, Energy Reports, ISSN 2352-4847, Elsevier, Amsterdam, Vol. 6, pp. 1160-1169, https://doi.org/10.1016/j.egyr.2020.05.002

Energy Reports 6 (2020) 1160–1169

Contents lists available at ScienceDirect

Energy Reports

journal homepage: www.elsevier.com/locate/egyr

Research paper

Nano carbides-mediated acceleration of energy release behavior of amorphous boron during ignition and combustion

Daolun Liang [a,*], Jianzhong Liu [b], Qili Qiu [c]

[a] Key Laboratory of Energy Thermal Conversion and Control of Ministry of Education, School of Energy and Environment, Southeast University, Nanjing 210096, China
[b] State Key Laboratory of Clean Energy Utilization, Zhejiang University, Hangzhou 310027, China
[c] School of Environmental Engineering, Nanjing Institute of Technology, Nanjing, 211167, China

ARTICLE INFO

Article history:
Received 11 February 2020
Received in revised form 7 April 2020
Accepted 1 May 2020
Available online xxxx

Keywords:
Nano-carbides
Amorphous boron
Heterogeneous combustion
Energy release behavior
Emission spectrum
Combustion temperature

ABSTRACT

Action mechanism of nano titanium carbide (nTiC), nano zirconium carbide (nZrC), and nano silicon carbide (nSiC) was studied using a concentrated ignition experimental system, an X-ray diffractometer and a scanning electron microscope. Each nano-carbide was mixed with B in mass ratio of 2/8 and then pressed into tablets, respectively. Furthermore, a sample of amorphous B was also prepared as the control group. All the three nano-carbides showed positive influence on the ignition of B. During the first stage of combustion, only nTiC could increase the maximum emission spectral intensity of the sample, while both nTiC and nZrC helped to increase that during the second stage of combustion. Although the addition of nano-carbides intensified the energy release rate of B (except nSiC), the expansion and diffusion of generated carbon dioxide took large amounts of heat away and reduced the surface temperature of the samples The temperature change in solid-phase exhibited a relationship with the spectral intensity change in gas-phase. The temperature increase was slow during the ignition delay stage, while the first combustion stage proceeded with rapid increase in surface temperature. The high-temperature areas regressed during the second combustion stage, accompanied by the gradual stopping of gas-phase reactions. The components and microstructure of the condensed combustion products (CCPs) were analyzed after the ignition experiment. Results showed that both nTiC and nZrC could react with B to generate corresponding metal borides, capable of promoting the ignition of B. Moreover, the catalysis of produced TiO_2 and ZrO_2 explain the increase of emission spectral intensity during the second combustion stage. A lot of micropores formed in the CCPs after adding nTiC, which showed a destructive effect of generated gaseous CO_2 on the surface oxide layer. In general, nTiC is the top accelerant for B oxidation in this study, while nSiC is at the bottom.

1. Introduction

Boron (B) is a potential substitute of metal fuel for solid propellant due to its excellent gravimetric and volumetric calorific values (58.86 kJ g^{-1} and 137.73 kJ cm^{-3}, respectively) (Haynes, 2014). However, the practical application of B is still under challenge because the difficulties encountered during its rapid ignition and full combustion have not yet been overcome (Gany and Timnat, 1993). At present, researchers have realized that the energy release behavior of B during combustion can be improved in the following three major ways: by shortening the ignition delay, catalyzing the oxidation, and breaking the surface oxide film (Eslami et al., 2008; Huang et al., 2019; Yeh and Kuo, 1996). For achieving these objectives, several attempts to find suitable additives for B have been made till date.

The ignition temperature of B is higher than most other metal fuels (Solomon et al., 2016), which causes a longer ignition delay. One effective method to promote B ignition involves the use of additive with lower ignition temperature. The pre-ignition of the additive can lead to the increase in the surrounding temperature and help to heat up B particles rapidly. Active metals, alloys, and explosives which have low ignition temperature and high energy density including magnesium, titanium, magnalium, hexogen, octogen, and so on can be used as "pre-ignition additives" (Liu et al., 2014b; Rosenband et al., 1995; Liu et al., 2014a; Liang et al., 2017a). These pre-ignition additives can effectively improve the ignition of B. However, most of them lost their benefits during the subsequent combustion stages.

According to the B combustion model provided by Yeh and Kuo (1996), the dominant combustion mechanism of B depends on value of Damkohler number (Da), defined as (E1):

$$\mathrm{Da} = \frac{Pd_0}{75} \tag{E1}$$

* Corresponding author.
E-mail address: ldl@seu.edu.cn (D. Liang).

https://doi.org/10.1016/j.egyr.2020.05.002

where P is the ambient pressure/atm and d_0 is the initial diameter of B/μm. If Da ≪ 1, the combustion reaction is mainly controlled by chemical kinetics; if Da = 1, the combustion is controlled by both chemical kinetics and oxygen diffusion; and if Da ≫ 1, the combustion is mainly controlled by oxygen diffusion. For most combustion processes of micro-sized B at atmospheric pressure, Da stays below 1. Therefore, catalysts can effectively accelerate the combustion by reducing the activation energy of oxidation. The most commonly used catalysts for B combustion are metal oxides, such as copper oxide (CuO), bismuth oxide (Bi_2O_3), iron oxide (Fe_2O_3), cerium oxide (CeO), and so on (Huang et al., 2019; Xi et al., 2013). Sometimes, metals can also be used as they can be readily oxidized during the combustion (Chintersingh et al., 2018).

Production and accumulation of oxide film on the surface of B particles is another obstacle for B combustion (Bidabadi et al., 2018). The surface oxide film, which is mainly formed by boron oxide (B_2O_3), has a low melting point (450 °C) and a high boiling point (1860 °C). As a result, the surface oxide film remains in liquid state during ignition and early combustion stages of B, and thus seriously hinders the permeation of ambient oxygen on particle surface (Liang et al., 2017a). Previous researches (Liu et al., 1996; Liang et al., 2016) have confirmed that the surface oxide film can be broken by gases such as carbon dioxide (CO_2), ammonia (NH_3), and water vapor (H_2O), generated during the combustion. Thus, additives which can be decomposed or oxidized to release gaseous products during combustion are also highly desirable.

Noteworthy, carbides have been used as solid propellant ingredients in the past several decades (Fox, 1962; Cohen and Zimmerman, 1975; Suri et al., 2010). However, their effects as additives for B combustion have rarely been reported. Most carbides have ignition temperature lower than that of B; therefore, they can be effectively used as the "pre-ignition additives". Moreover, corresponding oxides are produced during the combustion of carbides, including the solid part and the gaseous CO_2. The produced solid oxides may act as the catalyst for B oxidation, while CO_2 can help to break the surface oxide film on B particles. Therefore, suitable carbides may act as perfect additives for B combustion.

The main objectives of the present study are as follows: to find suitable carbides as accelerants for B combustion in order to reveal their acceleration mechanism on energy release behavior of B combustion. Nano-scaled carbide samples were used due to their higher reactivity than that of micro-scaled samples. Three different nano-carbides, namely, nano titanium carbide (nTiC), nano zirconium carbide (nZrC), and nano silicon carbide (nSiC) were mixed with amorphous B particles in mass ratio of 2/8, respectively. Moreover, an amorphous B sample without any additive was also prepared as the control group. A concentrated ignition experimental system was set up for the ignition experiments. The entire ignition and combustion processes of the samples were monitored using a fiber optic spectrometer and a thermal infrared imager in real-time. The condensed combustion products (CCPs) were collected and analyzed by an X-ray diffractometer (XRD) and a scanning electron microscope (SEM).

2. Experimental

2.1. Materials

The amorphous B used in this study was provided by Baoding Zhongpuruituo Technology Co., Ltd., China. The nano-carbides reagents were purchased from Aladdin Industrial Co., China. The purity and median particle size of all the reagents are listed in Table 1.

For each mixture sample, one of the above-mentioned nano-carbides was mechanically mixed with the amorphous B in mass ratio of 2/8 using a planetary mixer for 20 min to ensure the uniformity of the sample. The amorphous B (control group) and the mixture samples were then formed into cylindrical tablets using a manual tablet press. The diameter of the tablet was 8 mm, the thickness was 1.5 mm, and the average packing fraction was 47%. Prior to the test, each sample tablet was placed on a square tungsten slice with edge length of 30 mm and thickness of 1 mm, as shown in Fig. 1.

Table 1
Physical parameters of the obtained materials.

Sample	B	nTiC	nZrC	nSiC
Purity/%	99	99	99	99.9
Median particle size/nm	3400	50	50	40

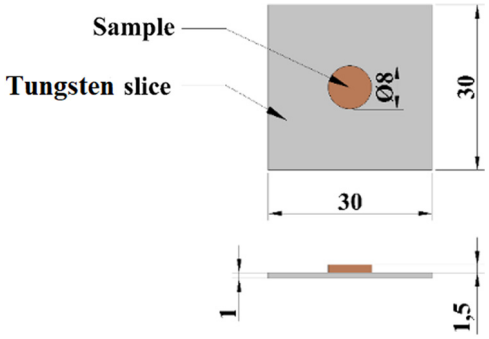

Fig. 1. Sample and tungsten slice.

In this study, the mass ratio, packing fraction, tablet size and shape were set empirically for laboratory experiments, which might not be the optimum values for practical applications.

2.2. Devices and methods

Schematic illustration of the concentrated ignition experimental system is presented in Fig. 2. The system contains the following four modules: a pressure chamber module, a xenon lamp ignition module, a combustion diagnosis module, and a control module. Further details about the experimental system are described in our previous literature report (Liang et al., 2017b).

In this study, power of the xenon lamp ignitor was set at 7 kW, and the maximum operating temperature in the combustor was measured to be approximately 800 °C. Oxygen gas with a flow rate of 6 L min^{-1} was used as the reaction gas, and the operating pressure was set at 1 atm. The fiber-optics probe of the fiber optic spectrometer (AvaSpec, Netherlands, AvaSpec-3648-USB2) was fixed in one of the measuring holes on the chamber body. The frame rate and measuring period of the fiber optic spectrometer were, respectively, set to 250 fps and 14 s. The integration time of the fiber optic spectrometer was approximately equal to the inverse of frame rate (4 ms) as the readout time for each spectrum (∼87 μs) is short enough to be ignored. Moreover, the thermal infrared imager (FLIR, the USA, T650sc) aimed at the sample tablets through the zinc selenide (ZnSe) glass window on the chamber body. The measuring range of the thermal infrared imager was 200–2100 °C. The function of infrared window compensation was turned on with a transmittance of 68% according to the glass characteristics. The emissivity was set to 0.87, the frame rate was 30 fps, and the measuring period was 12 s. The on–off of the measuring devices were synchronously controlled using a xenon lamp igniter. The tests were repeated 3 to 5 times to ensure the repeatability, and the standard deviations of results were presented in the form of error bars.

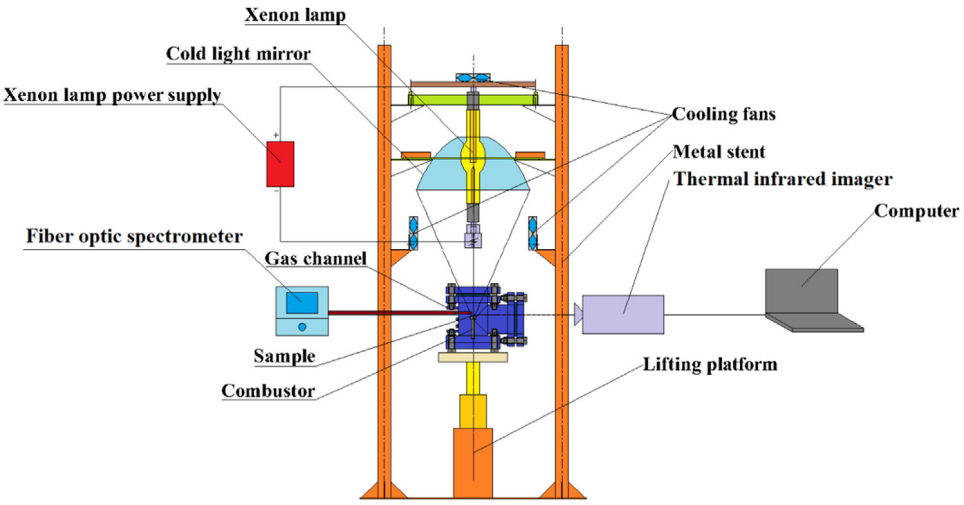

Fig. 2. Concentrated ignition experimental system.

The emissivity parameter used for the thermal infrared imager was measured based on the Tungsten wire method described in reference (Florko and Vovchuk, 2010). Firstly, the sample powders were coated on the upper half part of a Tungsten wire uniformly. Secondly, the Tungsten wire was heated under inert atmosphere to a high temperature range (800 to 1000 °C). As the emissivity of Tungsten is well known over a wide range of temperatures, its surface temperature (the lower half without coating) can be measured using a two-color infrared thermo detector (Changzhou Luming, China, LM-6108). Meanwhile, the actual temperature of the coated powders was assumed to be same as that of Tungsten during the inert heating. Then, the thermal infrared imager was aimed at the upper half part of the Tungsten wire and the emissivity parameter on the operating system was adjusted until the temperature reading equaled to that of the thermo detector. The final adjusted emissivity parameter was the measured surface emissivity of the sample. For the four samples used in this study, the measured surface emissivity values are all similar during the temperature range, and the average was 0.87. This result was similar to but a bit higher than previous measuring results of amorphous boron (Florko and Vovchuk, 2010; Hsieh and Yeh, 1993), which was attributed to the addition of nano carbides.

An XRD (PANalytical X'Pert PRO, Netherlands) was used for the component analysis of the CCPs. The sample tablets were placed right side up during the detection, and the diffraction angle range was 10–90°. In addition, a SEM (FEI SU-70, Japan) was used for the microstructure analysis of the CCPs. To protect the sample tablets from crushing, the CCPs were firstly immersed into an embedding kit (SPI Spurr, USA) and stored at 70 °C for 12 h. Thereafter, the embedding kit was cut to reveal the cross section of CCPs.

3. Results and discussion

3.1. Analysis of combustion spectra

Fig. 3 exhibits the maximum emission spectra obtained during the combustion (average results of multiple repeated tests). The spectral intensity represents the degree of violent nature of the oxidation reaction and energy release rate. Results showed that the B+nTiC sample exhibited the largest maximum emission spectral intensity among the four samples, while the B+nSiC showed the minimum intensity. The theoretical calorific values of the three nano-carbides are lower than that of B; therefore, higher oxidation ratios are required for the mixture samples to display larger maximum emission spectral intensity than amorphous B. Thus, nTiC can significantly promote the oxidation of B. The maximum emission spectral intensity of the B+nZrC sample is very close to that of amorphous B, which indicates that nZrC is also helpful to increase the oxidation ratio of B, though its effect is not as strong as that of nTiC.

Moreover, characteristic peaks of BO_2 (a gaseous intermediate product of B oxidation) and sodium (Na, an impurity in B sample) (Spalding et al., 1997) can be observed in the maximum emission spectral curves. The main source of BO_2 (as shown in (R1)) is a summation of (R1) to (R4) (Yeh and Kuo, 1996), which can be simplified in the form of a direct reaction between B and oxygen (O_2) (as expressed by (R5)) (Liang et al., 2017b; Burkholder and Andrews, 1991). The spectral signal of BO_2 has been used for judging the ignition of B in several previous studies (McNesby et al., 2015; Ao et al., 2014b). Moreover, (R5) is accompanied by huge amount of heat release, and thus the emission spectral intensity of BO_2 can reflect the oxidation and energy release rate of B as well. For the samples investigated herein, change rules of the leading characteristic peak of BO_2 (at 547.3 nm) were analyzed to compare the general trend of ignition and combustion processes.

$$B(s) + B_2O_3(1) \rightarrow 3/n(BO)_n(1) \quad (R1)$$

$$1/n(BO)_n + O_2(g) \rightarrow BO_2(a) + O(a) \quad (R2)$$

$$BO_2(a) + 1/n(BO)_n \rightarrow B_2O_3(1) \quad (R3)$$

$$O(a) + 1/n(BO)_n \rightarrow BO_2(g) \quad (R4)$$

$$B + O_2 \rightarrow BO_2,\ \triangle H = -861.9\ \text{kJ mol}^{-1} \quad (R5)$$

Fig. 4 shows the measured emission spectral intensity curves of the sample tablets at 547.3 nm (average results of multiple repeated trials), which exhibits the ignition and combustion of B in the sample tablets. Results show that the ignition and combustion process of a sample tablet can be divided into the following four stages: First, the spectral intensity of the sample tablets is maintained at a low level (around 10.0k counts) after the xenon lamp igniter is turned on; second, the spectral intensity increases

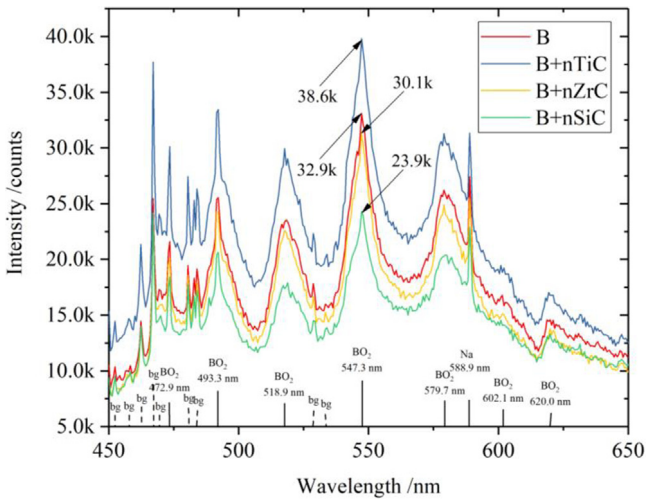

Fig. 3. Maximum emission spectra of the sample tablets ("bg" peaks are background light signals of the xenon lamp ignitor which should be ignored).

rapidly after the sample tablet is ignited, but attenuates again in a few moments; third, the spectral intensity gradually increases once again and sustains for a longer duration until the sample tablet extinguishes; and finally, the spectral intensity returns back and it is maintained at a low level until the measurement is completed.

The on–off of the fiber optic spectrometer was synchronously controlled using the xenon lamp igniter; therefore, the duration of the first stage is equal to the ignition delay time (t_{id}) of the sample tablet. The second and third stages are two continuous combustion stages, which were divided by a decline of emission spectral intensity. Similar two stage combustion phenomena of B were observed by Gan et al. (2012) in their earlier experiments. According to the classical theory of B combustion (Yeh and Kuo, 1996), the main cause of reduction in emission spectral intensity between the two stages is exactly the accumulation of surface oxide film. The oxidation of B proceeded rapidly after the ignition of sample tablet; however, the evaporation of surface oxide film was much slower. As a result, the liquid surface oxide film started to accumulate on the tablet surface and slowed down the oxidation reaction. However, owing to the continuous input of external energy (from the xenon lamp), the evaporation of liquid surface oxide film gradually increased, and the oxidation reaction was accelerated. Thus, initiation of the second combustion stage was enabled. To further compare the effect of different nano-carbides, the durations of the two stages were respectively defined as t_{c1} and t_{c2}, while the maximum emission spectral intensity of the two stages were respectively defined as I_{max1} and I_{max2} . The detailed values of the above-mentioned characteristic parameters are listed in Table 2.

As mentioned above, nano-carbides can be ignited before B as they have lower ignition temperatures. The pre-ignition of the

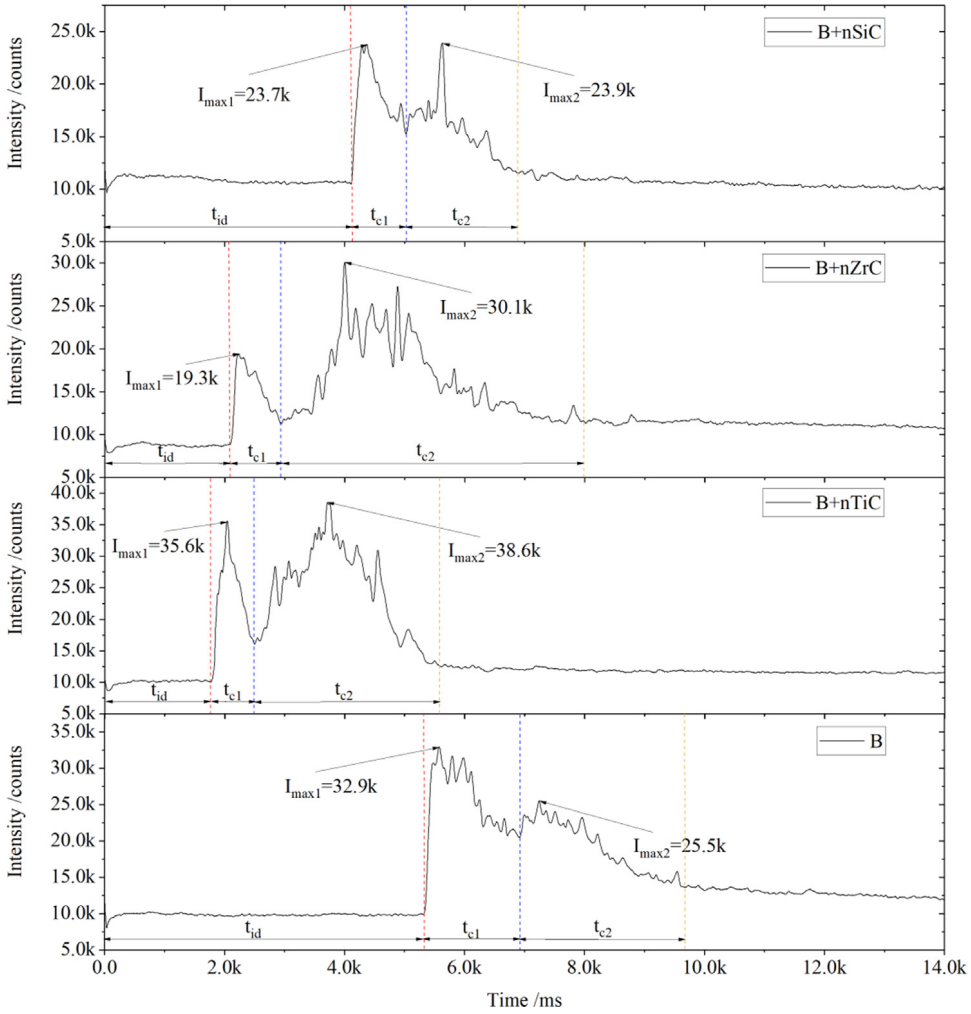

Fig. 4. Emission spectral intensity curves of the sample tablets at 547.3 nm.

Table 2
Characteristic parameters of the sample tablets during ignition and combustion.

Sample	t_{id}/ms	t_{c1}/ms	I_{max1}/counts	t_{c2}/ms	I_{max2}/counts
B	5336 ± 220	1608 ± 244	32.9k ± 1.7k	2712 ± 620	25.5k ± 0.9k
B+nTiC	1788 ± 136	672 ± 184	35.6k ± 2.0k	3104 ± 628	38.6k ± 1.9k
B+nZrC	2092 ± 296	848 ± 118	19.3k ± 1.0k	5044 ± 840	30.1k ± 1.2k
B+nSiC	4112 ± 124	916 ± 72	23.7k ± 1.5k	1852 ± 352	23.9k ± 1.3k

nano carbides released heat and lifted the sample temperature, and thus accelerated the ignition of boron. Therefore, all the mixture samples, in particular nTiC, have smaller t_{id} than amorphous B.

For the first combustion stage, t_{c1} can also be shortened by adding the nano-carbides. However, only the B+nTiC sample showed higher I_{max1} than amorphous B, which indicates that only nTiC led to the increase in the oxidation rate of B during the first combustion stage. The value of t_{c1} depends mainly on the accumulation rate of surface oxide film, while the accumulation rate of surface oxide film depends on both the combustion temperature and oxidation rate of B. A low combustion temperature is adverse to the evaporation of surface oxide film, and a high oxidation rate leads to rapid increase in its production. All the three nano-carbides released CO_2 during the combustion (which would take away the heat during gas expansion and diffusion); however, only nTiC could increase the oxidation rate of B at the same time, which explains why t_{c1} of the B+nTiC sample was the shortest among all the samples.

For the second combustion stage, both nTiC and nZrC showed positive influence on the oxidation rate of B, but nSiC exhibited the opposite trend. This result can be attributed to the catalytic action of TiO and ZrO (see details in Section 3.3), while SO_2 is usually considered to be inactive during B oxidation (Yeh and Kuo, 1996; Ao et al., 2014a). Furthermore, values of t_{c2} of the B+nTiC and B+nZrC samples are both larger than that of amorphous B. It should be noticed here the longer t_{c2} does not mean a lower combustion rate since the sample tablets did not burn out thoroughly during the experiments. As the experimental operating temperature was much lower than boiling point of B_2O_3, the final extinguishing of the sample tablets was caused by accumulation of the surface oxide film rather than complete oxidation, and the total quantity of burnt boron varied for different samples. As a result, the higher combustion and energy release rates corresponding to a higher I_{max2} value because only a higher reaction rate leaded to the instantaneous generation of more intermediate oxidation products. The longer t_{c2} values of the two samples actually mean they had higher burn-off ratios than amorphous boron. Therefore, higher I_{max2} and longer t_{c2} are both desired to achieve better energy release properties. Among the three nano-carbides used in this study, nTiC is the most beneficial to increase the oxidation rate and nZrC is the most beneficial to prolong the duration of the second combustion stage.

I_{max1} of amorphous B is larger than I_{max2}, which shows that the oxidation rate during the first stage is higher than that during the second stage. However, I_{max2} exceeds I_{max1} after the addition of nano-carbides, which indicates that the effect of the nano-carbides mainly came into role during the second stage of combustion. The addition of nTiC realized superior performance in both the ignition and combustion stages. It is found to be the best accelerant for energy release of B in this study.

3.2. Analysis of combustion temperature

The combustion temperature recorded using thermal infrared imager actually provided surface temperature data of the sample tablets. Noteworthy, the combustion temperature is unequal to, and often lower than the flame temperature in the gas phase region.

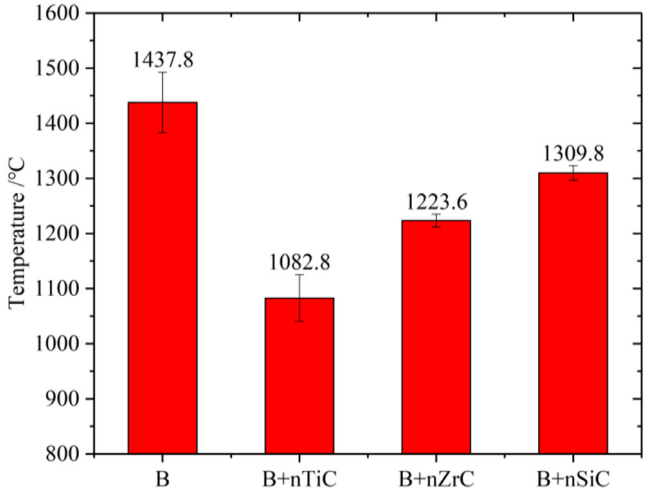

Fig. 5. Maximum surface temperature of the sample tablets during combustion.

The maximum surface temperature values of the sample tablets are presented in Fig. 5. Results indicate that the maximum surface temperature of amorphous B is the highest, while that of the B+nTiC sample is the lowest. Also, nZrC showed inferior effect on the combustion temperature of B than nTiC, and even less for nSiC. As mentioned above, the decrease of maximum surface temperature is a result of heat loss caused by CO_2 expansion and diffusion. Under our experimental conditions, the heat in gas phase was not utilized (or measured), which resulted in a simply decrease of surface temperature. However, this will not cause negative effects in a real rocket motor, where the heat in gas phase can transform into work through the gas expansion. Moreover, since the local temperature around boron particles can be much higher than the gas temperature, the ablation of motor walls may occur without a timely heat transfer to gas phase. Therefore, a relatively low surface temperature of fuel agglomerates is desired with the same energy release efficiency in practical applications. Therefore, the B+nTiC sample is still optimal as it exhibits both the low combustion temperature and good energy release behavior.

Based on the above-mentioned analysis, the surface temperature profile analysis focused on the B+nTiC sample, and the amorphous B sample was still set as the control group.

Fig. 6 exhibits the two-dimensional temperature profiles of the two samples with time interval of 1 to 2 s. Surface temperature of the sample tablets started to increase after the xenon lamp ignitor was turned on. The surface of the tablet was not completely smooth; therefore, the temperature increase was asynchronous everywhere. First, only some small areas on the tablet surface warmed up. Then the heat gradually spread to the surrounding areas as time passed. The light from the xenon lamp came from the upward side of the combustor; therefore, the high-temperature areas were generally distributed in the upper

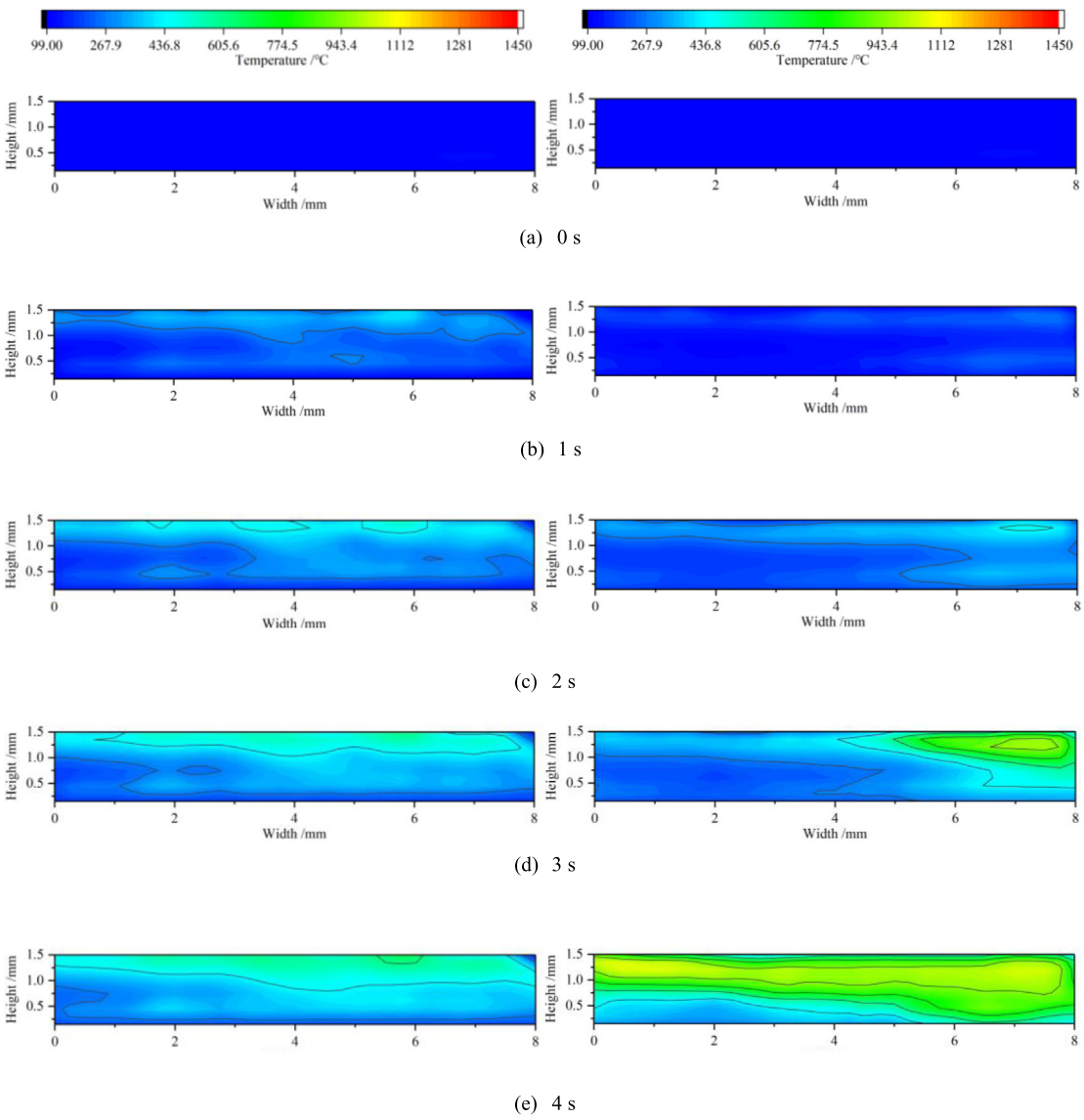

Fig. 6. Two-dimensional temperature profiles of the sample tablets (left: B, right: B+nTiC).

part of the sample tablets during the initial stage of combustion. With the continuation of the combustion process, the high-temperature areas gradually moved down to the center part of the sample tablets, which indicated declination of oxidation on the upper part and regression of the main reaction areas. However, the main reaction areas did not reach the bottom during the combustion, which can be attributed to the resistance due to accumulated oxidation products on the upper part. Actually, the accumulated oxidation products played a negative influence on the exchange of both heat and mass between unreacted B and the surroundings (Yeh and Kuo, 1996).

Fig. 6 shows the change rules of surface temperature on the sample tablets as well. Again, the entire process can be divided into three different stages. The temperature increase was slow at the beginning. For the amorphous B sample, this stage lasted from 0 to approximately 4 s. For the B+nTiC sample, this stage lasted from 0 to approximately 2 s. Results show the duration of the slow temperature-increase stage is relevant to that of the ignition delay stage. The sample tablets then passed into a rapid temperature-increase stage, during which the surface temperature values rapidly increased to the respective maximum. The duration of this stage lasted from approximately 4 to 6 s for the amorphous B sample, and approximately 2 to 4 s for the B+nTiC sample, which is relevant to that of the first combustion stage above. Finally, the surface temperature decreased gradually, which is relevant to the second combustion stage. Significant correlation was observed between the combustion stages divided based on the temperature profiles (mainly refer to solid-phase reactions) and those divided based on the emission spectral curves (mainly refer to gas-phase reactions). However, results show that the solid-phase and gas-phase reactions were not strictly in synchronization. During the slow temperature-increase stage, the solid-phase reaction already began, while the gas-phase reaction occurred barely. The first combustion stage started as the temperature-increase speeded up, and it came to an end along with the regression of the high-temperature areas. At the completion of the combustion, the gas-phase reaction stopped before the surface temperature reduced to the surrounding environmental temperature.

The temperature profiles of the other two mixture samples also showed similar change rules, thus they are not discussed in detail herein.

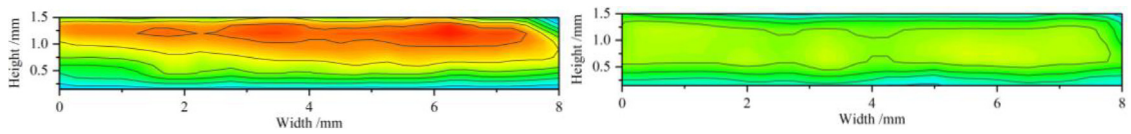

(f) 5 s

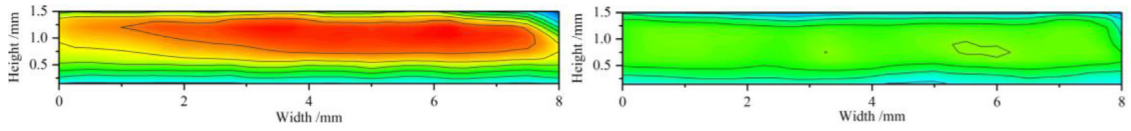

(g) 6 s

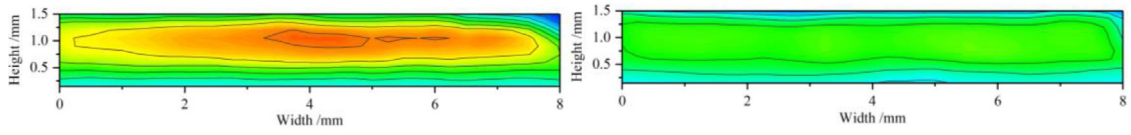

(h) 8 s

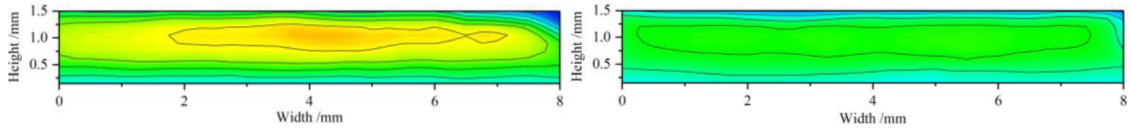

(i) 10 s

Fig. 6. (*continued*).

3.3. Analysis of condensed combustion products components and microstructure

After the ignition experiment, CCPs of the four samples were allowed to cool down naturally under inert atmosphere. An XRD was used for the component analysis of the residual sample tablets, and the result is presented in Fig. 7. Owing to the insensitivity of XRD to amorphous materials, unreacted amorphous B in the combustion residues was not detected.

B_2O_3 was found in the CCPs of all samples, as the final oxidation product of B. Furthermore, there was an incomplete oxidation product of B ($B_{13}O_2$) in the CCPs of amorphous B, which shows that the sample tablet was not burnt out during the experiment.

Analysis of the CCPs of the B+nTiC and B+nZrC samples indicated the presence of both the corresponding metal oxides and metal borides. The existence of TiB_2 and ZrB_2 indicates that nTiC and nZrC can react with B during the combustion, which can be helpful to bring forward the ignition of B. The generated TiO_2 and ZrO_2 can act as catalysts for B oxidation, which can explain the increase of emission spectral intensity during the second combustion stage as mentioned above. The cyclic reduction of TiO_2 can be expressed as (R2) and (R3), while that of ZrO_2 can be expressed as (R4) and (R5).

$$10B(s) + 3TiO_2(s) \rightarrow 3TiB_2(s) + 2B_2O_3(1) \quad (R2)$$

$$2TiB_2(s) + 5O_2(g) \rightarrow 2TiO_2(s) + 2B_2O_3(1) \quad (R3)$$

$$10B(s) + 3ZrO_2(s) \rightarrow 3ZrB_2(s) + 2B_2O_3(1) \quad (R4)$$

$$2ZrB_2(s) + 5O_2(g) \rightarrow 2ZrO_2(s) + 2B_2O_3(1) \quad (R5)$$

Fig. 7 does not show the existence of peaks of SiO_2, which can be attributed to the fact that the generated SiO_2 in the CCPs of B+nSiC sample was also amorphous. Moreover, SiC and 6H-SiC were detected, which indicates that the oxidation ratio of nSiC was not high during the combustion. Therefore, nSiC is not suitable for acceleration of B oxidation.

SEM images of the CCPs of amorphous B and B+nTiC samples were taken in order to compare their microstructure, and the results were displayed in Fig. 8.

The surface oxide film was found to be dense in the CCPs of amorphous B sample, while a lot of micropores existed in the CCPs of B+nTiC sample. The difference provides a strong evidence for the destructive effect of generated gaseous CO_2 on the surface oxide layer.

4. Conclusions

This study investigated the three different nano-carbides (nTiC, nZrC, and nSiC)-mediated acceleration of energy release behavior of amorphous B during ignition and combustion. Combustion spectra, combustion temperature, and CCPs component analyses were carried out to explore their action mechanism. The main findings of this study are summarized as follows:

(1) Emission spectra of the sample tablets were recorded using a fiber optic spectrometer. Characteristic peaks of BO_2 and impurity Na were detected. Characteristic peak intensity at 547.3 nm (the leading characteristic peak of BO_2) was used to reflect the oxidation and energy release rates of B. The ignition and combustion process of the sample tablet

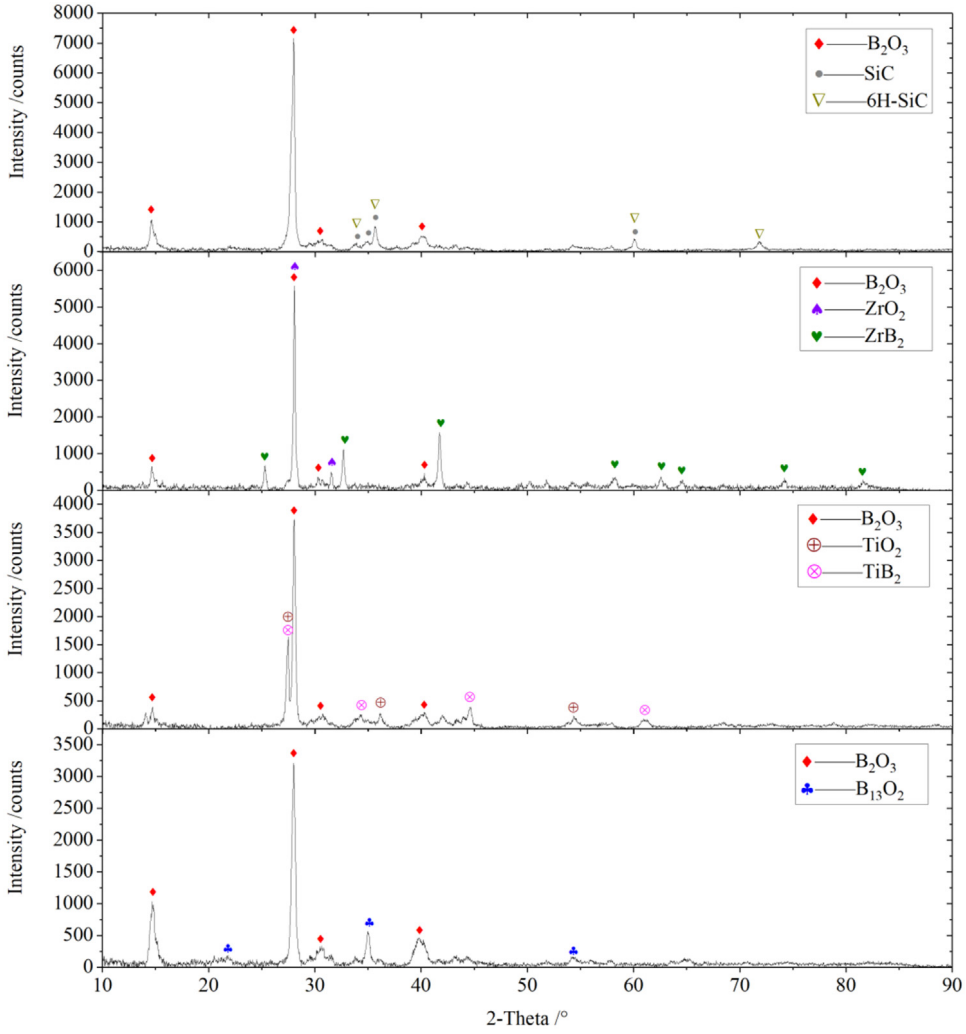

Fig. 7. XRD patterns of the CCPs of the samples.

included an ignition delay stage and two continuous combustion stages. Addition of all the three nano-carbides led to the shortening of the ignition delay of the samples. However, only nTiC increased the maximum emission spectral intensity during the first combustion stage. For the second combustion stage, both nTiC and nZrC showed positive influence on the oxidation rate of B, while nSiC exhibited the opposite trend.

(2) Surface temperature of the sample tablets was measured using the thermal infrared imager. The maximum surface temperature significantly decreased after adding the nano-carbides, especially nTiC. The temperature increase was asynchronous on the sample tablets, thus only some small areas on the tablet surface warmed up at first. During the early stage of combustion, the main reaction areas were distributed in the upper part of the sample tablets. As combustion proceeded, the main reaction areas gradually regressed to the center. The temperature change in solid-phase showed a relationship with the spectral intensity change in gas-phase. The temperature increase was slow during the ignition delay stage; however, increased rapidly during the first combustion stage. The high-temperature areas regressed during the second combustion stage, accompanied by the gradually stopping of gas-phase reactions.

(3) Component analysis of the CCPs was carried out using an XRD. $B_{13}O_2$ was detected in the CCPs of amorphous B, indicating the incompletion of the oxidation of B. Corresponding metal borides were found in the B+nTiC and B+nZrC samples, which can be an evidence for promoting B ignition. Moreover, corresponding metal oxides were found in these two samples, which can act as catalysts for B oxidation. In the B+nSiC sample, unoxidized SiC and 6H-SiC were detected as a result of low oxidation ratio of nSiC. SEM images were taken to show the difference in microstructure of the CCPs. The surface oxide film was dense in the CCPs of amorphous B sample, while a lot of micropores existed in those of B+nTiC sample due to the destructive effect of generated gaseous CO_2 on the surface oxide layer. In summary, nTiC can act as an effective accelerant for B oxidation and nZrC also has a certain positive effect; however, nSiC seems to have a negative influence when used as a B additive. In further research, more detailed action mechanism and key influence factors on accelerating B oxidation with nTiC need to be studied, including the effects of particle size, addition ratio, blending technique, and so on.

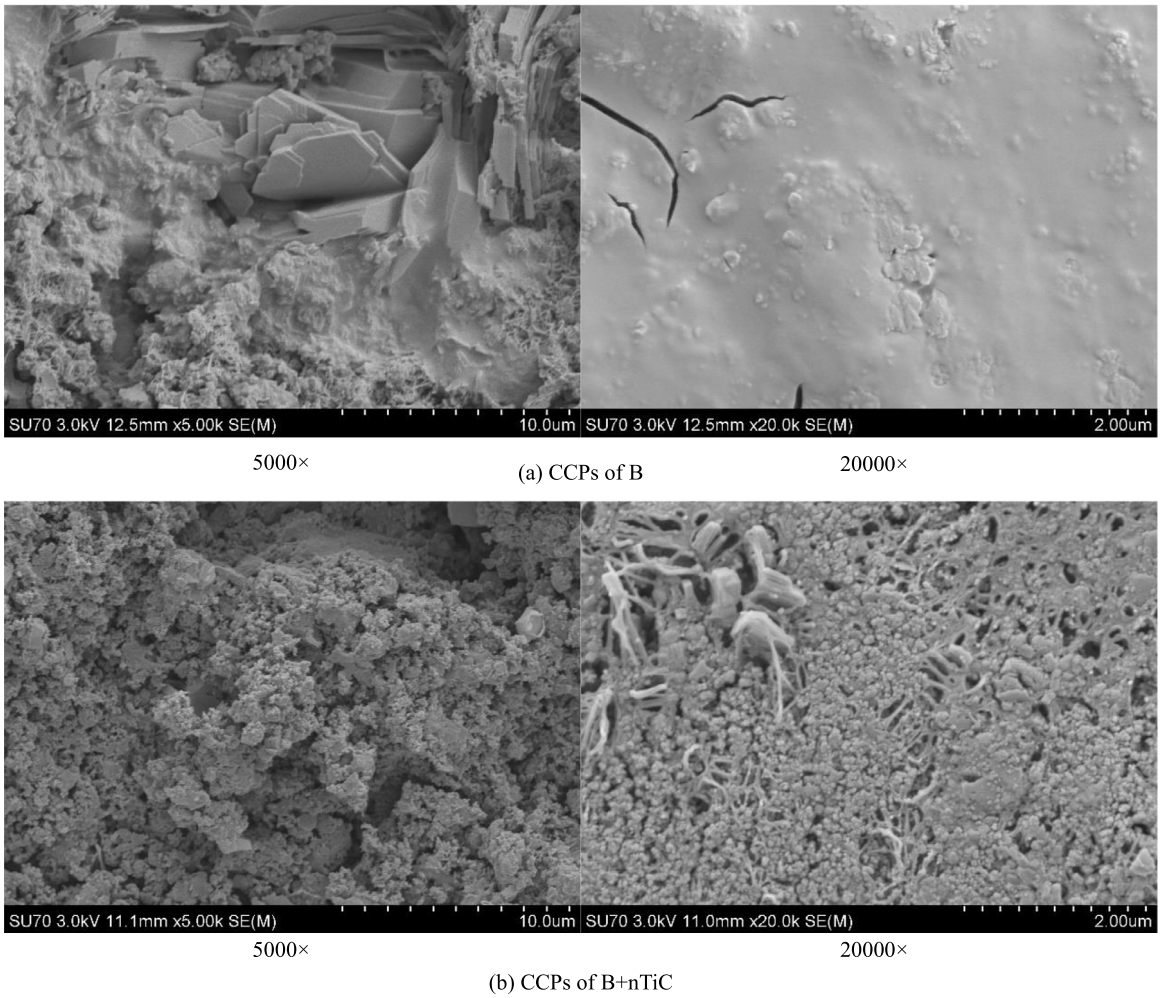

Fig. 8. SEM images of the CCPs of the samples.

CRediT authorship contribution statement

Daolun Liang: Project administration, Investigation, Data curation, Formal analysis, Visualization, Writing - original draft. **Jianzhong Liu:** Supervision, Conceptualization, Methodology, Writing - review & editing. **Qili Qiu:** Investigation, Data curation, Visualization, Writing - review & editing.

Declaration of competing interest

The authors declare that they have no known competing financial interests or personal relationships that could have appeared to influence the work reported in this paper.

Acknowledgments

This work was financially supported by the National Natural Science Foundation of China (No. 51906040) and the Fundamental Research Funds for the Central Universities, China (No. 2242019K40013).

References

Ao, W., Yang, W., Wang, Y., et al., 2014a. Ignition and combustion of boron particles at one to ten standard atmosphere. J. Propul. Power 30 (3), 760–764.

Ao, W., Zhou, J.H., Yang, W.J., et al., 2014b. Ignition, combustion, and oxidation of mixtures of amorphous and crystalline boron powders. Combust. Explos. Shock Waves 50 (6), 664–669.

Bidabadi, M., Bozorg, M.V., Bordbar, V., et al., 2018. Flame propagation through heterogeneous combustion of hybrid aluminum-boron poly-disperse particle suspensions in air. Fuel 215, 714–725.

Burkholder, T.R., Andrews, L., 1991. Reactions of boron atoms with molecular oxygen. Infrared spectra of BO, BO_2, B_2O_2, B_2O_3, and BO- 2 in solid argon. J. Chem. Phys. 95 (12), 8697–8709.

Chintersingh, K.L., Schoenitz, M., Dreizin, E.L., 2018. Combustion of boron and boron–iron composite particles in different oxidizers. Combust. Flame 192, 44–58.

Cohen, J., Zimmerman, G.A., 1975. Solid propellants with stability enhanced additives of particulate refractory carbides or oxides: U.S. patent 3, 924, 405. pp. 12–19.

Eslami, A., Hosseini, S.G., Pourmortazavi, S.M., 2008. Thermoanalytical investigation on some boron–fuelled binary pyrotechnic systems. Fuel 87 (15–16), 3339–3343.

Florko, A.V., Vovchuk, Y.I., 2010. Emissivity characteristics of boron and boric oxide at high temperatures. Combust. Explos. Shock Waves 46 (2), 178–182.

Fox, H.M., 1962. Gelled nitroalkane propellants: U.S. patent 3, 035, 948. pp. 5–22.

Gan, Y., Lim, Y.S., Qiao, L., 2012. Combustion of nanofluid fuels with the addition of boron and iron particles at dilute and dense concentrations. Combust. Flame 159 (4), 1732–1740.

Gany, A., Timnat, Y.M., 1993. Advantages and drawbacks of boron-fueled propulsion. Acta Astronaut. 29 (3), 181–187.

Haynes, W.M., 2014. CRC Handbook of Chemistry and Physics. CRC press.

Hsieh, W.H., Yeh, C.L., 1993. Approach to the measurement of burning-surface temperature of boron. J. Propuls. Power 9 (1), 157–160.

Huang, S., Deng, S., Jiang, Y., et al., 2019. Experimental effective metal oxides to enhance boron combustion. Combust. Flame 205, 278–285.

Liang, D., Liu, J., Chen, B., et al., 2016. Improvement in energy release properties of boron-based propellant by oxidant coating. Thermochim. Acta 638, 58–68.

Liang, D., Liu, J., Zhou, Y., et al., 2017a. Ignition and combustion characteristics of amorphous boron and coated boron particles in oxygen jet. Combust. Flame 185, 292–300.

Liang, D., Liu, J., Zhou, Y., et al., 2017b. Ignition and combustion characteristics of molded amorphous boron under different oxygen pressures. Acta Astronaut. 138, 118–128.

Liu, L., He, G., Wang, Y., 2014a. Effect of oxidizer on the combustion performance of boron-based fuel-rich propellant. J. Propul. Power 30 (2), 285–289.

Liu, T.K., Shyu, I.M., Hsia, Y.S., 1996. Effect of fluorinated graphite on combustion of boron and boron-based fuel-rich propellants. J. Propul. Power 12 (1), 26–33.

Liu, J., Xi, J., Yang, W., et al., 2014b. Effect of magnesium on the burning characteristics of boron particles. Acta Astronaut. 96, 89–96.

McNesby, K.L., Biss, M.M., Benjamin, R.A., et al., 2015. Chemical imaging of explosions–mapping BO2 light emission. Propellants, Explos. Pyrotech. 40 (4), 539–543.

Rosenband, V., Natan, B., Gany, A., 1995. Ignition of boron particles coated by a thin titanium film. J. Propul. Power 11 (6), 1125–1131.

Solomon, Y., Grinstein, D., Natan, B., 2016. Active boron dispersion and ignition in gel droplet. Int. J. Energ. Mater. Chem. Propuls. 15 (3), 197–213.

Spalding, M.J., Krier, H., Burton, R.L., 1997. Emission spectroscopy during ignition of boron particles at high pressure. In: 35 Th AIAA Aerospace Sciences Meeting and Exhibit. pp. 97–0119.

Suri, A.K., Subramanian, C., Sonber, J.K., et al., 2010. Synthesis and consolidation of boron carbide: a review. Metall. Rev. 55 (1), 4–40.

Xi, J., Liu, J., Wang, Y., et al., 2013. Metal oxides as catalysts for boron oxidation. J. Propul. Power 30 (1), 47–53.

Yeh, C.L., Kuo, K.K., 1996. Ignition and combustion of boron particles. Prog. Energy Combust. Sci. 22 (6), 511–541.